AMERICAN SOCIETY FOR MICROBIOLOGY | Journal of Bacteriology®

RESEARCH ARTICLE

Synergy between c-di-GMP and Quorum-Sensing Signaling in *Vibrio cholerae* Biofilm Morphogenesis

Jojo A. Prentice,[a] Andrew A. Bridges,[a] Bonnie L. Bassler[a,b]

[a]Department of Molecular Biology, Princeton University, Princeton, New Jersey, USA
[b]The Howard Hughes Medical Institute, Chevy Chase, Maryland, USA

ABSTRACT Transitions between individual and communal lifestyles allow bacteria to adapt to changing environments. Bacteria must integrate information encoded in multiple sensory cues to appropriately undertake these transitions. Here, we investigate how two prevalent sensory inputs converge on biofilm morphogenesis: quorum sensing, which endows bacteria with the ability to communicate and coordinate group behaviors, and second messenger c-di-GMP signaling, which allows bacteria to detect and respond to environmental stimuli. We use *Vibrio cholerae* as our model system, the autoinducer AI-2 to modulate quorum sensing, and the polyamine norspermidine to modulate NspS-MbaA-mediated c-di-GMP production. Individually, AI-2 and norspermidine drive opposing biofilm phenotypes, with AI-2 repressing and norspermidine inducing biofilm formation. Surprisingly, however, when AI-2 and norspermidine are simultaneously detected, they act synergistically to increase biofilm biomass and biofilm cell density. We show that this effect is caused by quorum-sensing-mediated activation of *nspS-mbaA* expression, which increases the levels of NspS and MbaA, and in turn, c-di-GMP biosynthesis, in response to norspermidine. Increased MbaA-synthesized c-di-GMP activates the VpsR transcription factor, driving elevated expression of genes encoding key biofilm matrix components. Thus, in the context of biofilm morphogenesis in *V. cholerae*, quorum-sensing regulation of c-di-GMP-metabolizing receptor levels connects changes in cell population density to detection of environmental stimuli.

IMPORTANCE The development of multicellular communities, known as biofilms, facilitates beneficial functions of gut microbiome bacteria and makes bacterial pathogens recalcitrant to treatment. Understanding how bacteria regulate the biofilm life cycle is fundamental to biofilm control in industrial processes and in medicine. Here, we demonstrate how two major sensory inputs—quorum-sensing communication and second messenger c-di-GMP signaling—jointly regulate biofilm morphogenesis in the global pathogen *Vibrio cholerae*. We characterize the mechanism underlying a surprising synergy between quorum-sensing and c-di-GMP signaling in controlling biofilm development. Thus, the work connects changes in cell population density to detection of environmental stimuli in a pathogen of clinical significance.

KEYWORDS biofilm morphogenesis, *Vibrio cholerae*, c-di-GMP, quorum sensing, signal transduction

Bacteria often integrate multiple sensory cues into the control of behaviors, including the formation of biofilms—surface-associated bacterial communities encapsulated in self-produced extracellular matrices (1). The biofilm lifestyle confers advantages to constituent members, including protection against antibiotics, predation, and shear stress (2–4). Indeed, biofilms are a predominant form of bacterial life in the environment, in industrial processes, and in disease (5).

In the global pathogen and model biofilm-forming bacterium *Vibrio cholerae*, two well-studied sensory inputs control the biofilm life cycle. The first is quorum sensing, a

Editor George O'Toole, Geisel School of Medicine at Dartmouth

Address correspondence to Bonnie L. Bassler, bbassler@princeton.edu.

The authors declare no conflict of interest.

Received 25 June 2022
Accepted 31 August 2022
Published 26 September 2022

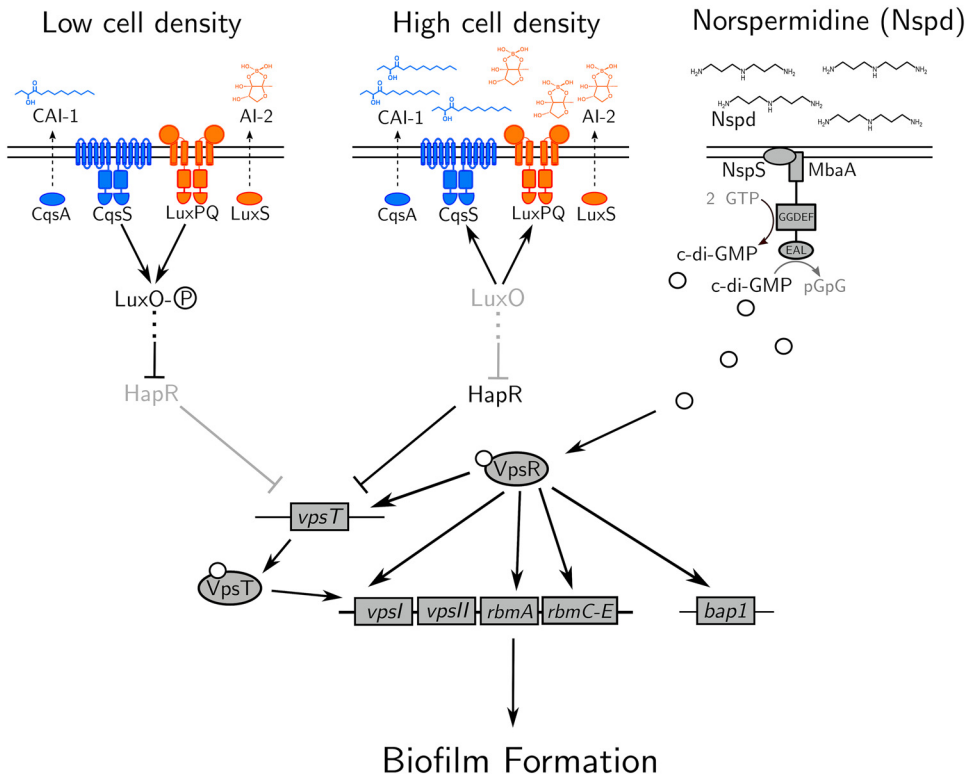

FIG 1 Model showing the contributions of quorum-sensing and norspermidine signaling to biofilm gene expression. See text for details. The P in the circle represents phosphate. White circles represent c-di-GMP. Nspd, norspermidine.

cell-cell communication process that orchestrates collective behaviors (6). Quorum sensing relies on the production, release, and group-wide detection of extracellular signaling molecules called autoinducers (7). *V. cholerae* possesses five quorum-sensing autoinducer-receptor pairs, two of which are key to the present work, diagrammed in Fig. 1 (8). At low cell density, the autoinducer receptors CqsS and LuxPQ are unliganded and function as kinases, channeling phosphate to the response regulator LuxO (9, 10). Phosphorylated LuxO (LuxO~P) indirectly represses the gene encoding the high-cell-density master regulator HapR (11, 12). HapR represses expression of the vibrio polysaccharide biosynthetic genes encoded in the *vpsI* and *vpsII* operons, *vpsT*, encoding a transcriptional activator of the *vpsI* and *vpsII* operons, and *rbmA* and the *rbmC-E* operon, encoding biofilm matrix proteins. Thus, in the low-cell-density quorum-sensing regime, when *hapR* is repressed, VPS and biofilm matrix protein levels are high and *V. cholerae* forms biofilms (13). At high cell density, cholera autoinducer-1 (CAI-1) and autoinducer-2 (AI-2) accumulate and bind CqsS and LuxPQ, respectively, converting them from kinases to phosphatases. Phosphate is stripped from LuxO, which inactivates it (9, 10). As a result, HapR is produced, it suppresses biofilm formation, and biofilm dispersal occurs (Fig. 1) (12).

The second major regulator of the *V. cholerae* biofilm life cycle is the second messenger molecule cyclic diguanylate (c-di-GMP). c-di-GMP is produced and degraded by enzymes containing diguanylate cyclase and/or phosphodiesterase activities, respectively. These activities are commonly modulated by environmental stimuli, including light, temperature, amino acids, oxygen, and polyamines (14–18). High intracellular c-di-GMP levels drive biofilm formation via binding to and activation of the VpsT and VpsR transcription factors. VpsT-c-di-GMP and VpsR-c-di-GMP both activate expression of the *vpsI* and *vpsII* operons, and additionally, VpsR-c-di-GMP activates expression of *rbmA*, *rbmC-E*, and *bap1*. In contrast, when cytoplasmic c-di-GMP levels are low, biofilm formation is repressed, favoring the motile state (Fig. 1) (18, 19). Thus, in *V. cholerae*, the low-cell-density quorum-sensing regime and high levels of cytoplasmic c-di-GMP

each promote biofilm formation, whereas the high-cell-density quorum-sensing regime and low levels of cytoplasmic c-di-GMP each repress biofilm formation. Attempts to knit together the *V. cholerae* quorum-sensing and c-di-GMP pathways have revealed two key findings: first, high cytoplasmic c-di-GMP concentrations can override negative quorum-sensing regulation of biofilm genes (20, 21). Second, the high-cell-density quorum-sensing regime activates the expression of genes encoding over a dozen diguanylate cyclases and phosphodiesterases, while repressing only a few genes encoding such enzymes (8, 20).

Here, we investigate the integration of quorum-sensing and c-di-GMP information in *V. cholerae* biofilm morphogenesis, from ligand detection to population-scale biofilm changes. We use exogenous administration of the AI-2 autoinducer to modulate quorum-sensing activity, and we use administration of the polyamine norspermidine to control the activity of the NspS-MbaA c-di-GMP-metabolizing circuit (Fig. 1) (17). We find that, as expected, quorum sensing represses biofilm formation in the absence of NspS-MbaA detection of norspermidine. However, surprisingly, quorum sensing increases biofilm biomass and biofilm cell density when MbaA-mediated c-di-GMP synthesis is stimulated by norspermidine supplementation. We show that this positive quorum-sensing effect occurs because at high cell density, HapR activates *nspS-mbaA* expression, which drives increased NspS and MbaA production and, consequently, increased c-di-GMP production when the norspermidine ligand is present. The increased c-di-GMP activates VpsR, which in turn, activates *rbmA* matrix gene expression, resulting in the formation of larger and denser biofilms. We propose a model in which quorum sensing represses biofilms but also primes the bacterial population to optimally respond to environmental stimuli that foster c-di-GMP production. Our findings reveal a new mechanism by which *V. cholerae* modulates its biofilm life cycle, and moreover, they show that quorum sensing does not strictly repress *V. cholerae* biofilm formation.

RESULTS

Quorum sensing elevates norspermidine-driven increases in biofilm biomass in *V. cholerae*. To investigate how *V. cholerae* integrates information from c-di-GMP and quorum-sensing signaling into the control of the biofilm life cycle, we measured biofilm phenotypes across quorum-sensing and c-di-GMP signaling regimes. To simplify the regulation of quorum sensing, we used a *V. cholerae* strain harboring only a single quorum-sensing receptor that controls LuxO phosphorylation—the AI-2 receptor LuxPQ. Moreover, we deleted the AI-2 synthase *luxS* so that quorum sensing is exclusively controlled through exogenous administration of AI-2. We refer to this strain as the "AI-2-responsive strain." First, we measured biofilm biomass accumulation over time in the AI-2-responsive strain in the absence of AI-2 (i.e., in the low-cell-density quorum-sensing regime [Fig. 2A and B]). Consistent with previous findings, in this signaling regime, biofilms formed (Fig. 2A) (13). Addition of saturating AI-2 (i.e., to achieve the high-cell-density quorum-sensing regime [Fig. 2A and B]) prevented the AI-2-responsive strain from forming biofilms, again consistent with previous findings (13, 20, 22). To investigate how changes in c-di-GMP affect biofilm formation in the low- and high-cell-density quorum-sensing regimes, we provided exogenous norspermidine to drive c-di-GMP production. Norspermidine had only a modest effect on peak biofilm biomass when the AI-2-responsive *V. cholerae* strain was in the low-cell-density quorum-sensing regime, whereas surprisingly, norspermidine drove dramatically increased biofilm biomass when the strain was in the high-cell-density quorum-sensing regime (Fig. 2A and B). These results were independent of the specific autoinducer-receptor pair used to stimulate quorum sensing in *V. cholerae*, as we likewise modulated quorum sensing in a CAI-1-responsive strain and obtained analogous results (Fig. S1A).

To assess whether the combination of the CAI-1 and AI-2 cues altered the balance between quorum-sensing repression of biofilm gene expression and quorum-sensing synergy with norspermidine, we supplemented a strain that is responsive to both CAI-1 and AI-2 (i.e., that lacks both *cqsA* and *luxS*) with norspermidine, the CqsS agonist, and

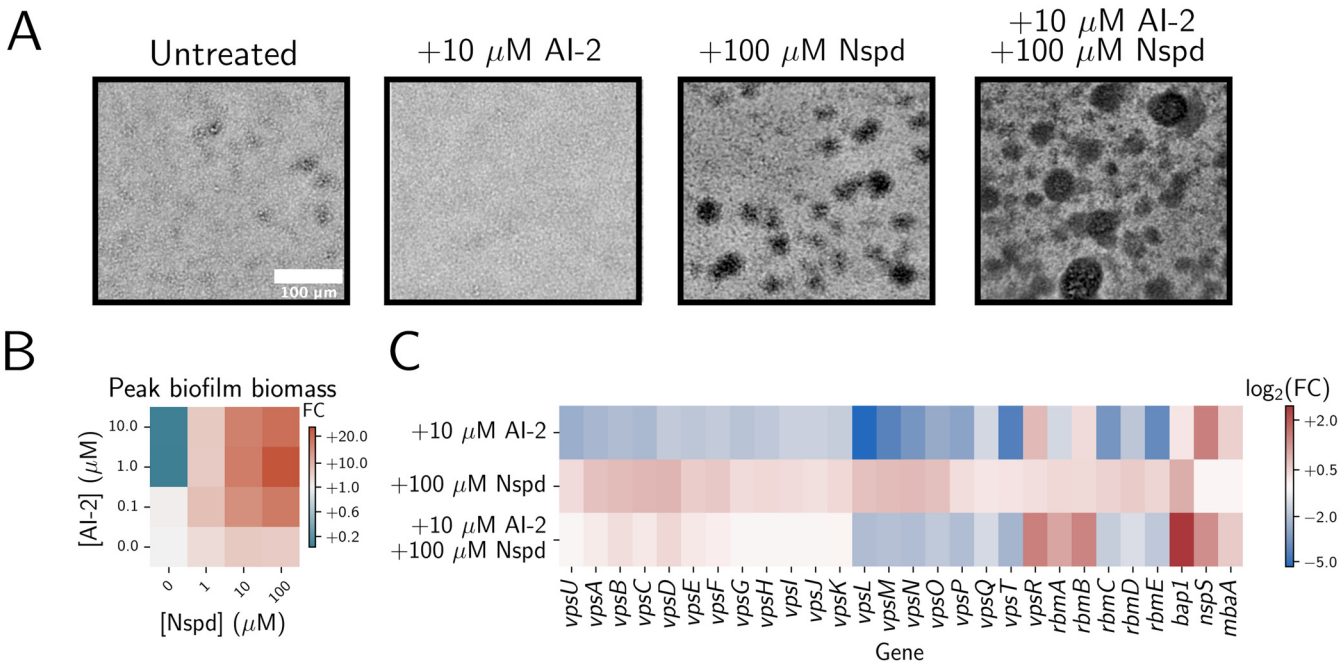

FIG 2 Quorum sensing elevates norspermidine-mediated increases in biofilm biomass in *V. cholerae*. (A) Representative bright-field images of biofilms produced by the *V. cholerae* AI-2-responsive strain after 14 h of growth with the indicated treatments. (B) Quantitation of peak biofilm biomass for the AI-2-responsive strain grown with the indicated treatments, displayed as a heatmap. Data are normalized as fold changes relative to the untreated AI-2-responsive strain (bottom-left corner). (C) Heatmap of $\log_2$ fold changes in biofilm gene expression in the AI-2-responsive strain grown with the indicated treatments normalized to that of the untreated strain. Samples were collected at an OD_{600} of 0.1. Nspd, norspermidine; FC, fold change.

AI-2 and measured the effects on biofilm biomass. The triple combination resulted in roughly equivalent biofilm biomass accumulation, as did supplementation with norspermidine and AI-2 in the AI-2-responsive strain (Fig. S1B). Thus, we conclude that the synergy between quorum-sensing and norspermidine signaling is a general feature of the high-cell-density quorum-sensing regime.

Crucially, biofilm biomass did not increase in the high-cell-density quorum-sensing and high-norspermidine regime when *mbaA* was deleted (Fig. S1C). This result shows that changes in biofilm biomass are mediated by the known polyamine-sensing NspS-MbaA pathway. Thus, although quorum sensing and norspermidine independently drive opposing biofilm phenotypes, with quorum sensing repressing and c-di-GMP promoting biofilm formation, together, they function synergistically to increase biofilm biomass in *V. cholerae*.

To define the gene expression changes underlying the quorum-sensing and norspermidine signaling synergy in *V. cholerae* biofilm morphogenesis, we conducted RNA sequencing (RNA-seq) in the AI-2-responsive strain under each condition shown in Fig. 2A. Treatment with AI-2 alone drove a reduction in *vps* operon, *vpsT*, *rbmA*, and *rbmC-E* expression, consistent with previous findings and with repression of biofilm formation (Fig. 2C) (20, 23). Conversely, treatment with norspermidine caused a modest elevation in *vps* operon and *bap1* expression (Fig. 2C). Simultaneous treatment with AI-2 and norspermidine reduced *vps* operon, *vpsT*, and *rbmC-E* expression and increased *vpsR*, *rbmA*, and *bap1* expression. These results suggest that quorum sensing and norspermidine act synergistically to elevate biofilm biomass through a mechanism that decouples *vps* polysaccharide biosynthesis gene expression from expression of genes encoding the matrix proteins RbmA and Bap1.

HapR activates *nspS-mbaA* expression at high cell density, which increases both c-di-GMP production and biofilm biomass in response to norspermidine. To explore the unexpected result that quorum sensing enhances norspermidine-driven increases in biofilm biomass in *V. cholerae*, we began by measuring the effects on c-di-GMP—the immediate output of the MbaA circuit in response to norspermidine. To do this, we

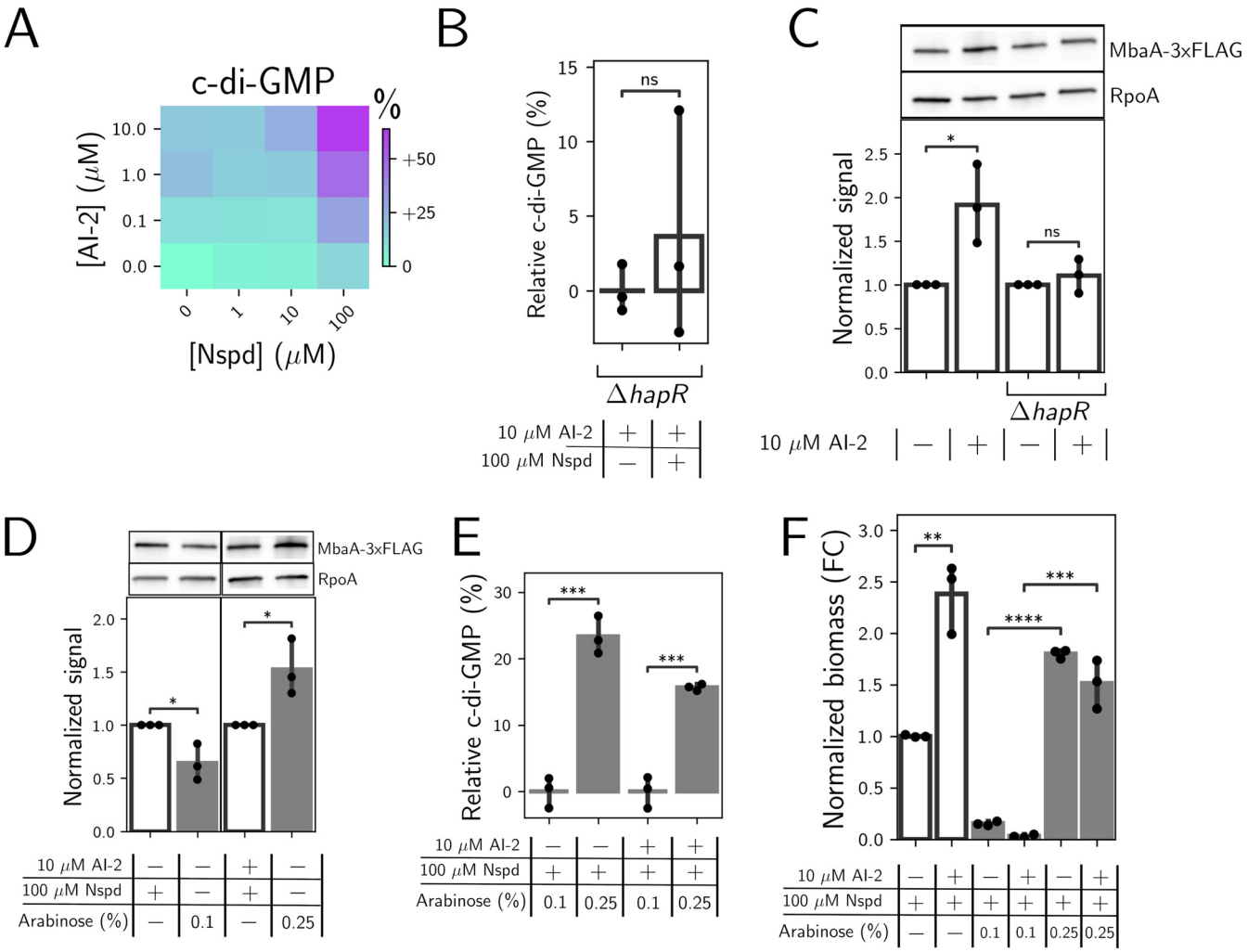

FIG 3 HapR-mediated activation of *nspS-mbaA* expression drives quorum-sensing and norspermidine synergy in c-di-GMP and biofilm biomass production. (A) c-di-GMP reporter output in the AI-2-responsive strain following the indicated treatments, shown as a heatmap. Data are displayed as percent differences compared to the untreated strain (bottom-left corner), with teal representing low and purple representing high c-di-GMP reporter output. (B) c-di-GMP reporter output in the Δ*hapR* AI-2-responsive strain following the indicated treatments. Data are normalized as percent changes relative to the Δ*hapR* AI-2-responsive strain treated with AI-2 (left bar). *N* = 3 biological replicates. (C) (Top panel) Western blot of MbaA-3xFlag in the AI-2-responsive strain and the Δ*hapR* AI-2-responsive strain following the indicated treatments. (Bottom panel) Quantitation of MbaA-3×Flag protein levels from the top panel. Data are normalized as fold changes relative to the AI-2 treatment in each strain and in each replicate. *N* = 3 biological replicates. (D) (Top panel) Western blot of MbaA-3×Flag in the AI-2-responsive strain (1st and 3rd lanes) and the AI-2-responsive strain carrying *Pbad-nspS-mbaA* on the chromosome (2nd and 4th lanes), treated as indicated. (Bottom panel) Quantitation of MbaA-3×Flag protein levels from the top panel. Data in the first and second bars are normalized to data in the first bar for each replicate. Data in the third and fourth bars are normalized to data in the third bar for each replicate. *N* = 3 biological replicates. (E) c-di-GMP reporter output in the AI-2-responsive strain carrying *Pbad-nspS-mbaA* on the chromosome. Data are normalized as percent changes relative to the mean c-di-GMP output for the 0.1% arabinose treatment for each group. *N* = 3 biological replicates. (F) Quantitation of peak biofilm biomass for the AI-2-responsive strain and the AI-2-responsive strain carrying *Pbad-nspS-mbaA* on the chromosome, treated as indicated. Images were taken at 14 h. Data are normalized as fold changes (FC) relative to the AI-2-responsive strain grown with norspermidine. *N* = 3 biological replicates. In panels D to F, white bars show results for the AI-2-responsive strain, and gray bars show results for the AI-2-responsive strain carrying *pbad-nspS-mbaA-3×Flag*. In panels B to F, unpaired *t* tests were performed for statistical analyses. ****, $P \leq 0.0001$; ***, $P \leq 0.001$; **, $P \leq 0.01$; *, $P \leq 0.05$; ns $P > 0.05$. Nspd, norspermidine; FC, fold change.

employed a fluorescent, riboswitch-based reporter of c-di-GMP levels (24, 25). Surprisingly, although provision of AI-2 alone repressed biofilm formation (Fig. 2A and B), c-di-GMP reporter output was modestly elevated in the high-cell-density quorum-sensing state (Fig. 3A). We considered possible roles for quorum-sensing master regulators in modulating c-di-GMP levels. It is known that the HapR high-cell-density master transcription factor drives c-di-GMP degradation, eliminating it as a candidate (Fig. 1) (25). Thus, we suspected that the low-cell-density quorum-sensing master regulators—the Qrr1-4 small RNAs and/or the AphA transcription factor—could reduce c-di-GMP levels at low cell density. If so, repression of the low-cell-density master regulators at high cell density could underpin

the increase in c-di-GMP that occurs following AI-2 treatment. Deletion of *aphA* in a low-cell-density-locked mutant strain (encoding the phosphomimic *luxO*^{D61E} allele), also lacking *hapR* (*luxO*^{D61E} Δ*hapR*), increased c-di-GMP reporter output to the level of a high-cell-density-locked mutant strain (encoding a nonphosphorylatable LuxO allele) lacking *hapR* (*luxO*^{D61A} Δ*hapR*). Deletion of *qrr*1-4 in the Δ*aphA* Δ*hapR* strain had no additional effect on c-di-GMP reporter output (Fig. S2). We infer from these data that AphA, but not the Qrr sRNAs, suppresses c-di-GMP reporter output in the low-cell-density quorum-sensing state. Thus, both the low- and high-cell-density quorum-sensing master regulators reduce c-di-GMP levels, and high-cell-density repression of *aphA* expression explains how supplementation with AI-2 elevates c-di-GMP reporter output. Notably, however, the small increase in c-di-GMP that occurs following supplementation with AI-2 alone is insufficient to override HapR-mediated repression of *vpsT* and the *vps* operons. Hence, biofilm formation is repressed under this treatment condition. Finally, consistent with our biofilm measurements, simultaneous administration of norspermidine and AI-2 drove maximal c-di-GMP reporter output (Fig. 3A).

To explain how AI-2 supplementation could increase c-di-GMP levels when norspermidine is present, we posited that at high cell density, HapR could activate *nspS-mbaA* expression. Consequently, higher levels of NspS and MbaA would be produced, enabling increased synthesis of c-di-GMP and, in turn, increased biofilm biomass in response to norspermidine. Data supporting this possibility are the following: first, our RNA-seq results show that in the high-cell-density quorum-sensing regime, *nspS* and *mbaA* transcript levels are elevated (Fig. 2C). Second, a mathematical model that we previously developed to capture NspS-MbaA-mediated c-di-GMP production/degradation predicts that elevating NspS and MbaA concentrations should increase c-di-GMP in response to norspermidine (17). Third, in the Δ*hapR* AI-2-responsive strain, c-di-GMP output remained insensitive to the addition of norspermidine when AI-2 was supplied (Fig. 3B). Thus, a HapR-dependent mechanism must underlie the elevated sensitivity of the c-di-GMP reporter to norspermidine. To test our hypothesis, we tagged MbaA with 3×Flag and measured protein levels by Western blotting in the AI-2-responsive strain and in the Δ*hapR* AI-2-responsive strain in the presence and absence of AI-2. We did not measure NspS, because *nspS* and *mbaA* are in an operon, and we observed that both *nspS* and *mbaA* transcript levels increased in step in the high-cell-density quorum-sensing signaling state (Fig. 2C) (26). Indeed, MbaA levels doubled following AI-2 supplementation, and moreover, this increase depended on HapR (Fig. 3C).

To probe whether increasing NspS-MbaA levels is sufficient to promote the observed increase in the sensitivity of c-di-GMP biosynthesis to changes in norspermidine levels, we replaced the endogenous chromosomal *nspS-mbaA* promoter with the arabinose-controlled *Pbad* promoter, and additionally, we tagged MbaA with 3×Flag. Thus, we could synthetically modulate NspS-MbaA production by supplying arabinose, we could quantify MbaA levels by Western blotting, and we could track changes in c-di-GMP production. Importantly, this strategy provided the essential feature of removing quorum-sensing control of *nspS-mbaA* transcription. We identified a concentration of arabinose (0.1%) that drove MbaA production to roughly the level achieved by norspermidine treatment alone (Fig. 3D). We likewise identified a concentration of arabinose (0.25%) that produced the doubling in MbaA production that occurs following norspermidine and AI-2 cotreatment (Fig. 3D). Companion measurements of c-di-GMP reporter output showed that increasing NspS and MbaA levels drove increased c-di-GMP production (Fig. 3E) for samples grown with only norspermidine and with both norspermidine and AI-2. Consistent with this finding, increasing NspS and MbaA levels increased biofilm biomass accumulation to roughly the same extent in the presence of norspermidine alone and in the presence of both norspermidine and AI-2 (Fig. 3F). Thus, we conclude that HapR-directed activation of *nspS-mbaA* expression accounts for the increased sensitivity of c-di-GMP biosynthesis to norspermidine in the high-cell-density quorum-sensing regime. Moreover, the increased sensitivity of c-di-GMP biosynthesis to norspermidine results

in elevated biofilm biomass in the high-cell-density and high-norspermidine signaling regime.

Finally, we considered the possibility that an NspS-MbaA-independent mechanism could also contribute to the synergy between norspermidine and quorum-sensing signaling. For this analysis, we introduced the *vpvC*^{W240R} gene encoding a constitutively active diguanylate cyclase under the *Pbad* promoter onto the chromosome of the AI-2-responsive strain. This construct allowed us to ramp up intracellular c-di-GMP levels via arabinose treatment. In the high-cell-density quorum-sensing regime, no increase in biofilm biomass occurred at any level of *vpvC*^{W240R} expression within the range tested, suggesting that quorum sensing does not generally enhance the sensitivity of biofilm biomass to changes in c-di-GMP levels (Fig. S3). Rather, quorum sensing specifically enhances norspermidine-driven increases in biofilm biomass through an NspS-MbaA-directed enhancement in the sensitivity of c-di-GMP biosynthesis to norspermidine.

MbaA-synthesized c-di-GMP activates VpsR. We sought to identify the downstream component responsible for transducing the AI-2- norspermidine-driven increase in c-di-GMP into the control of biofilm biomass. We hypothesized that the increased c-di-GMP produced by MbaA could activate and/or increase the levels of the transcription factors VpsT and VpsR, both of which control expression of biofilm-related genes (23). Consistent with our RNA-seq results, VpsT-3×Flag and VpsR-3×Flag levels increased following supplementation with both norspermidine and AI-2 compared to supplementation with AI-2 alone, as did the downstream matrix protein, RbmA-3×Flag (we note, however, that the changes in VpsT-3×Flag and VpsR-3×Flag levels do not achieve statistical significance [Fig. 2C and Fig. S4]). Thus, we examined the individual roles of VpsT and VpsR in controlling RbmA protein levels. Regarding VpsT, in a Δ*vpsT* AI-2-responsive strain in the high-norspermidine and high-quorum-sensing signaling regime, the VpsR-3×Flag level was equivalent to that in the AI-2-responsive strain following the same treatment (Fig. S4). However, the Δ*vpsT* AI-2-responsive strain possessed lower RbmA-3×Flag than the AI-2-responsive strain in the high-norspermidine and high-quorum-sensing signaling regime (Fig. S4). Regarding VpsR, in the Δ*vpsR* AI-2-responsive strain, we could not detect VpsT-3×Flag or RbmA-3×Flag in the high-cell-density and high-norspermidine signaling state (Fig. S4). Together, these results suggest that VpsR regulates *vpsT* expression, but not vice versa, and both VpsR and VpsT independently regulate *rbmA* expression. Moreover, we infer that because VpsT does not regulate *vpsR* expression, the modest activation of *vpsR* expression that occurs in the high-norspermidine and high-quorum-sensing signaling regime is a consequence of VpsR autofeedback, as shown previously (27). We conclude that in the high-cell-density quorum-sensing and high-norspermidine signaling regime, HapR-mediated activation of *nspS-mbaA* increases norspermidine-driven c-di-GMP production. c-di-GMP, in turn, activates VpsR. The VpsR-c-di-GMP complex activates expression of the *vps* operons, *rbmA*, and to a lesser extent, *vpsR*. VpsR-c-di-GMP also indirectly activates these same genes via induction of *vpsT* expression and consequent VpsT-c-di-GMP-mediated transcriptional activation.

Activation of *rbmA* expression promotes alterations in biofilm morphogenesis in the high-cell-density and high-norspermidine signaling regime. To probe whether quorum-sensing and c-di-GMP signaling synergistically affect overall biofilm architecture, we compared the spatial characteristics of *V. cholerae* biofilms receiving no treatment, treatment with norspermidine, and treatment with both norspermidine and AI-2 using single-cell-resolution microscopy. We assessed the relation between cell distance from the biofilm core and local cell density (i.e., how tightly packed the cells are) for all cells in the biofilm under each signaling regime. Cells in biofilms treated with both ligands resided in closer proximity to one another at the biofilm core than cells in untreated biofilms or cells in biofilms treated with norspermidine alone (Fig. 4A to C and E). These results indicate that the high-norspermidine and high-cell-density quorum-sensing signaling state alters global biofilm architecture, leading to densification of the biofilm core.

Obvious candidates to connect norspermidine and quorum-sensing signaling to biofilm densification are the biofilm matrix proteins Bap1 and RbmA, as expression of

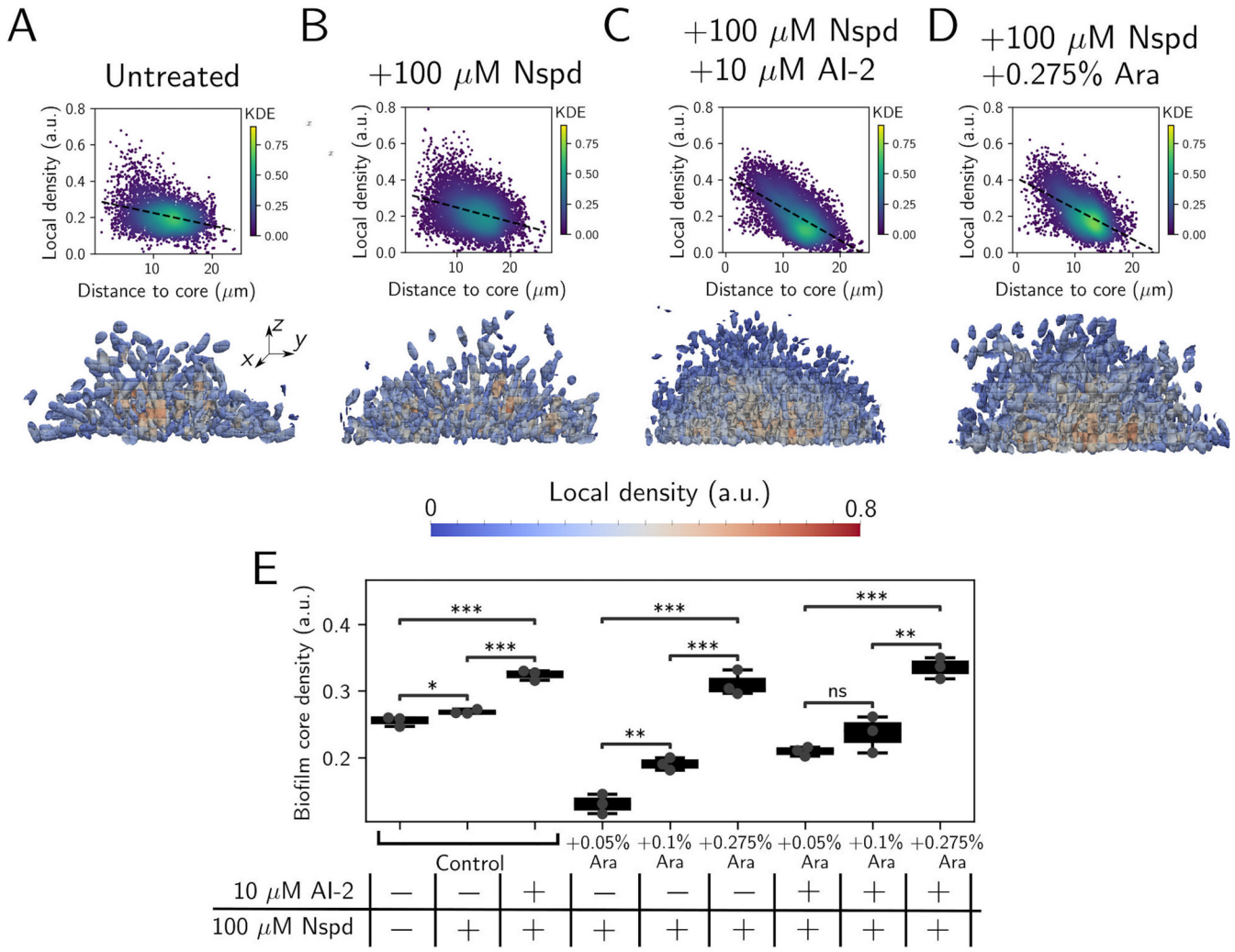

FIG 4 Norspermidine and quorum-sensing signaling jointly enhance biofilm biomass through RbmA-mediated biofilm core densification. (A to C) (Top panels) Scatterplots showing the relationship between local biofilm cell density and distance from the biofilm core in the AI-2-responsive strain, treated as indicated. (Bottom panels) Cross-sectional 3D renderings of segmented cells in biofilms ~16 h postinoculation, colored by local biofilm cell density and treated as in the top panels. (D) As in panels A to C for the Δ*rbmA* AI-2-responsive strain harboring chromosomal *Pbad-rbmA-3×Flag*, treated as indicated. (E) Box plot showing the biofilm core cell density in the AI-2-responsive strain (denoted "control") and the Δ*rbmA Pbad-rbmA-3×Flag* AI-2-responsive strain following the indicated treatments. Shown are the means ± standard deviations for $N = 3$ biological replicates. Unpaired *t* tests were performed for statistical analyses. In panels A to D, data points are colored by the kernel density estimate, which represents the probability density function with respect to local biofilm density and distance to the biofilm core. ****, $P \leq 0.0001$; ***, $P \leq 0.001$; **, $P \leq 0.01$; *, $P \leq 0.05$; ns, $P > 0.05$. Nspd, norspermidine; Ara, arabinose; KDE, kernel density estimate.

the genes encoding them is activated in the high-cell-density and high-norspermidine signaling regime (Fig. 2C). Following treatment with both ligands, the Δ*bap1* strain exhibited no change in bulk biofilm biomass or biofilm core density compared to the parent AI-2-responsive strain treated with both ligands, eliminating a role for Bap1 (Fig. S5A and B). In contrast, deletion of *rbmA* reduced peak biofilm biomass in the high-cell-density and high-norspermidine signaling regime (Fig. S5A). Moreover, upon washing, biofilms formed by the Δ*rbmA* AI-2-responsive strain detached from the substrate, likely because they were fragile due to decreased cell-cell adhesion (Fig. S5C) (28, 29). Synthetic induction of *rbmA* expression increased biofilm core density in a dose-dependent manner (Fig. 4E), consistent with previous results (30). Thus, ligand-driven *rbmA* upregulation is a potential mechanism that links the high-norspermidine and high-cell-density quorum-sensing signaling regime to changes in biofilm architecture. Indeed, when we matched RbmA-3×Flag levels in the norspermidine-treated Δ*rbmA* strain to the doubly ligand-treated parent strain using a chromosomal *Pbad-*

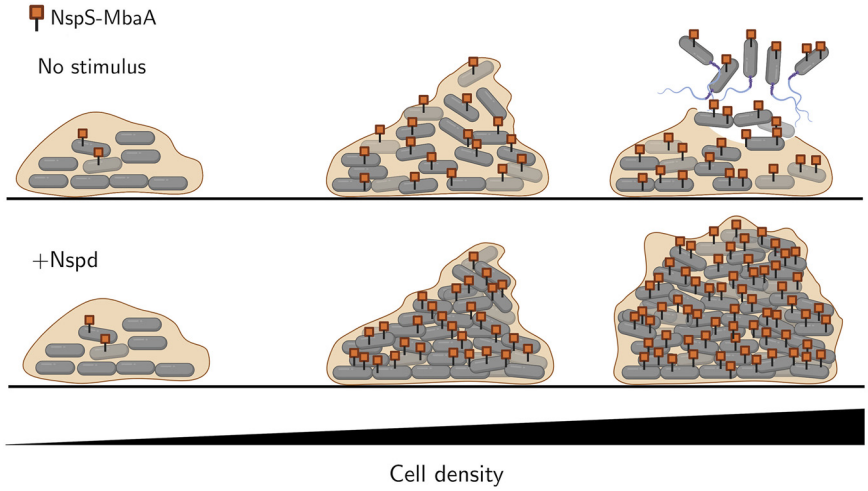

FIG 5 Proposed model for the integration of quorum-sensing and c-di-GMP signaling in *V. cholerae* biofilm morphogenesis. At low cell density, HapR levels are low, and consequently, NspS-MbaA levels are low, biofilm genes are expressed, and biofilms form. As the bacterial population grows and cell density increases, HapR levels rise, and HapR activates *nspS* and *mbaA* expression. (Top) At high cell density, in the absence of norspermidine, the NspS-MbaA circuit is inactive, and HapR-mediated repression of biofilm gene expression causes dispersal. (Bottom) At high cell density, in the presence of norspermidine, the NspS-MbaA pathway is activated, and high levels of the Nspd-NspS-MbaA complex produce c-di-GMP that increases biofilm gene expression, leading to biofilm expansion and densification. Nspd, norspermidine.

rbmA-3×Flag construct (using 0.275% arabinose; Fig. 4D), the spatial density correlations and the biofilm core densities of the two strains became roughly equivalent (Fig. 4C to E). Thus, increased *rbmA* expression largely explains the synergistic effects of norspermidine and quorum-sensing signaling on biofilm biomass accumulation.

DISCUSSION

In this study, we investigated the effects of simultaneously altering c-di-GMP and quorum-sensing signaling on *V. cholerae* biofilm morphogenesis. Strikingly, we found that changing c-di-GMP signaling through norspermidine supplementation had little effect on biofilm biomass in the low-cell-density quorum-sensing signaling state but had a biofilm-promoting effect in the high-cell-density quorum-sensing signaling state (Fig. 2). We demonstrated that the synergy between the signaling pathways is a consequence of increased production of NspS and MbaA at high cell density. Thus, under this condition, c-di-GMP levels can increase if norspermidine is present (Fig. 3). The effect of elevated c-di-GMP levels is activation of VpsR, which we infer undergoes positive feedback and activates *rbmA* and *vps* operon gene expression both directly and indirectly via induction of *vpsT* (Fig. 2 and Fig. S4). Notably, our RNA-seq results show that *vpsT* is most highly expressed in the presence of norspermidine alone, yet biofilm biomass is highest following norspermidine and AI-2 cotreatment. We infer that HapR-mediated repression is stronger than VpsR-mediated activation of *vpsT*, even when high levels of c-di-GMP are present. Nonetheless, when both ligands are present, the levels of VpsT and VpsR produced are sufficient to drive increased biofilm biomass. The combined changes in gene expression in the high-cell-density quorum-sensing and high-norspermidine signaling state drive the formation of larger, denser biofilms than those that form in the low-cell-density signaling state (Fig. 4). The major takeaway from this research is that, remarkably, quorum sensing can either promote or suppress biofilm biomass accumulation, depending on the presence or absence of environmental cues that impinge on c-di-GMP signaling (Fig. 5).

Our findings imply that quorum sensing confers plasticity to the population-level decision to commit to the biofilm or the free-swimming state. In the absence of c-di-GMP-modulating signals, quorum sensing promotes the free-swimming state at high

cell density, but via upregulation of c-di-GMP-metabolizing enzymes that detect environmental stimuli, quorum-sensing signaling has the potential to drive the opposite output behavior of population-level commitment to the biofilm state. It has long been known that quorum sensing controls the expression of genes encoding over a dozen c-di-GMP-metabolizing enzymes (Fig. S6) (20). However, the ramifications of this regulatory arrangement have remained mysterious prior to this work. A previously reported model for c-di-GMP and quorum-sensing integration proposed that quorum-sensing communication and detection of environmental stimuli such as oxygen, polyamines, nitric oxide, etc. independently contribute to alterations in c-di-GMP levels (31). Our results show that, at least for the quorum-sensing and polyamine cues, this is not the case. Rather, the stimuli act synergistically. Testing the generality of this model remains to be performed; however, the possibility to do so is limited by the scarcity of known ligands that control diguanylate cyclase and phosphodiesterase activities.

We wonder how the results presented here might extend to other bacteria. *V. cholerae* is unusual in that individually, the high-cell-density quorum-sensing state and the high-c-di-GMP state promote opposite biofilm phenotypes. In other bacteria, such as *Pseudomonas aeruginosa*, the high-cell-density quorum-sensing state and the high-c-di-GMP state both independently promote biofilm formation (32, 33). In *P. aeruginosa*, the prevailing model for c-di-GMP signaling and its influence on biofilm development is that c-di-GMP-metabolizing enzymes with specialized sensory functions in biofilm formation (e.g., surface sensing) are upregulated and/or activated at different points in the biofilm life cycle, typically via two-component signal transduction pathways (33). Thus, context-dependency is a known feature of c-di-GMP signaling in *P. aeruginosa* biofilm morphogenesis; however, connections between quorum sensing and environmental stimuli that promote changes in c-di-GMP levels and biofilm formation remain uncharacterized in *P. aeruginosa*. Probing the interactions between quorum-sensing and c-di-GMP signaling in *P. aeruginosa* and other species that occupy diverse niches and that have lifestyles that differ dramatically from that of *V. cholerae* could deliver a unified picture of how the coordination of sensory signaling systems is linked to the ecological and evolutionary roles that biofilms play across the bacterial domain.

MATERIALS AND METHODS

Bacterial strains, reagents, reporters, and Western blotting procedures. The *V. cholerae* strain used in this study was O1 El Tor biotype C6706str2. Antibiotics were used at the following concentrations: polymyxin B, 50 μg/mL; kanamycin, 50 μg/mL; spectinomycin, 200 μg/mL; chloramphenicol, 1 μg/mL; and gentamicin, 5 μg/mL. Strains were propagated at 30°C in liquid lysogeny broth (LB) with shaking or LB containing 1.5% agar for plates. Strains used for reporter assays, imaging assays, and RNA isolation were grown in M9 minimal medium supplemented with 0.5% dextrose, 0.5% Casamino Acids, and 0.1 mM boric acid. AI-2 (*S*-2-methyl-2,3,3,4-tetrahydroxytetrahydrofuran-borate) and the CqsS agonist 1-ethyl-*N*-{[4-(propan-2-yl)phenyl]methyl}-1*H*-tetrazol-5-amine were synthesized as described previously (34–37). Norspermidine (Millipore Sigma, I1006-100G-A), arabinose (Millipore Sigma, W325501), AI-2, and the CqsS agonist were added at the concentrations designated in the figures or figure legends at the initiation of the assay. c-di-GMP was measured as described previously (17, 25). Western blotting for MbaA-3×Flag, VpsT-3×Flag, VpsR-3×Flag, and RbmA-3×Flag were performed as described previously, using a monoclonal anti-Flag-peroxidase antibody (Millipore Sigma, no. A8592; Danvers, MA, USA). RpoA served as the loading control, and it was detected using an anti-*Escherichia coli* RNA polymerase α primary antibody (BioLegend, no. 663104) and an anti-mouse IgG horseradish peroxidase (HRP)-conjugated secondary antibody (Promega, no. W4021) (13). For strains carrying VpsT-3×Flag, RbmA-3×Flag, or VpsR-3×Flag, prior to application of the anti-RpoA antibody, the anti-Flag-peroxidase antibody was stripped from the membranes by incubation at 25°C in stripping buffer (15 g/L glycine, 1 g/L SDS, 10 mL/L Tween 20, diluted in water, buffered to pH 2.2) for 15 min, followed by a second incubation with stripping buffer for 10 min, followed by two 10-min incubations in phosphate-buffered saline (PBS), and finally, two 5-min incubations in PSB with Tween 20 (PBST).

DNA manipulation and strain construction. Modifications to the *V. cholerae* genome were generated by replacing genomic DNA with linear DNA introduced by natural transformation as described previously (13, 38, 39). PCR and Sanger sequencing (Genewiz) were used to verify genetic alterations. See Table S1 for primers and g-blocks (IDT) and Table S2 for a list of strains used in this study. Constructs driven by the *Pbad* promoter were introduced at the neutral locus *vc1807*. The *Pbad-nspS-mbaA* construct was produced by replacing the native *nspS* promoter with *Pbad*.

Microscopy analyses. Measurements of biofilm biomass were made as described previously (13) using bright-field microscopy with minimal modifications. In brief, single-plane images were acquired at 30-min intervals on a BioTek Cytation 7 multimodal plate reader using an air immersion 20× lens

objective (Olympus, PL FL; numerical aperture [NA], 0.45) with static incubation at 30°C. Analyses were performed using Fiji software version 1.53c. Images in the time series were smoothed using a Gaussian filter (σ = 10), followed by segmentation using an intensity threshold. The total amount of light attenuated in each image after segmentation was summed to yield the biofilm biomass for the corresponding time point.

For high-resolution images of cells in biofilms (Fig. 4 and Fig. S5), samples were fixed by treatment with 3.7% formaldehyde (Avantor, MFCD00003274) in PBS for 10 min. To terminate fixation, samples were washed five times with PBS. Cells were subsequently stained with 1 μg/mL 4′,6-diamidino-2-phenylindole (DAPI) in PBS for 30 min at 25°C. Single-cell-resolution images of fixed samples were acquired using a DMI8 SP-8 point scanning confocal microscope (Leica, Wetzlar, Germany) equipped with a 63× water immersion objective (Leica, HC PL APO CS2; NA, 1.20). The excitation light source was a 405-nm diode laser, and emitted light was detected by a GaAsP spectral detector (Leica, HyD SP). Cell segmentation and biofilm parameter calculations were performed using BiofilmQ (parameters Architecture_LocalDensity and Distance_ToBiofilm CenterAtSubstrate) (30). All plots were generated using Python version 3. Figures were assembled in Inkscape (40; https://inkscape.org/).

RNA isolation and sequencing. Overnight cultures of the *V. cholerae* AI-2-responsive strain, grown in biological triplicate, were diluted to an optical density at 600 nm (OD_{600}) of ~0.001 in 5 mL of M9 medium. The subcultured cells were grown at 30°C with shaking in the presence of the designated polyamine and/or AI-2 treatment to an OD_{600} of 0.1. Cells were harvested by centrifugation for 10 min at 4,000 rpm and resuspended in RNAprotect (Qiagen). RNA was isolated using the RNeasy minikit (Qiagen), remaining DNA was digested using the TURBO DNA-free kit (Invitrogen), and the concentration and purity of RNA were measured using a NanoDrop instrument (Thermo). Samples were flash-frozen in liquid nitrogen and stored at −80°C until they were shipped on dry ice to SeqCenter (https://www.seqcenter.com/rna-sequencing/). The 12 million paired-end reads option and the intermediate analysis package were selected for each sample. Quality control and adapter trimming were performed with bcl2fastq (Illumina), while read mapping was performed with HISAT2 (41). Read quantitation was performed using Subread's featureCounts (42) functionality, and subsequently, counts were loaded into R and normalized using the edgeR (43) trimmed mean of M values (TMM) algorithm. Values were converted to counts per million (cpm), and differential expression analyses were performed using the edgeR quasi-linear F-test (qlfTest) functionality against treatment groups, as indicated. The results, presented in Fig. 2C, were plotted using Python version 3 (40).

Data availability. The RNA-seq data can be found in Data Set S1 in the supplemental material.

SUPPLEMENTAL MATERIAL

Supplemental material is available online only.

SUPPLEMENTAL FILE 1, PDF file, 1.2 MB.

SUPPLEMENTAL FILE 2, XLSX file, 1.6 MB.

ACKNOWLEDGMENTS

We thank members of the Bassler group for insightful discussions. This work was supported by the Howard Hughes Medical Institute, NSF grant MCB-2043238, NIH grant 2R37GM065859 (B.L.B.), and NIH grant 1K99AI158939 (A.A.B.). The funders had no role in study design, data collection and analysis, decision to publish, or preparation of the manuscript.

REFERENCES

1. Flemming HC, Wingender J, Szewzyk U, Steinberg P, Rice SA, Kjelleberg S. 2016. Biofilms: an emergent form of bacterial life. Nat Rev Microbiol 14:563–575. https://doi.org/10.1038/nrmicro.2016.94.
2. Flemming HC, Wingender J. 2010. The biofilm matrix. Nat Rev Microbiol 8:623–633. https://doi.org/10.1038/nrmicro2415.
3. Mah T-F, Pitts B, Pellock B, Walker GC, Stewart PS, O'Toole GA. 2003. A genetic basis for Pseudomonas aeruginosa biofilm antibiotic resistance. Nature 426:306–310. https://doi.org/10.1038/nature02122.
4. Shaw T, Winston M, Rupp CJ, Klapper I, Stoodley P. 2004. Commonality of elastic relaxation times in biofilms. Phys Rev Lett 93:e098102.
5. Costerton JW, Stewart PS, Greenberg EP. 1999. Bacterial biofilms: a common cause of persistent infections. Science 284:1318–1322. https://doi.org/10.1126/science.284.5418.1318.
6. Mukherjee S, Bassler BL. 2019. Bacterial quorum sensing in complex and dynamically changing environments. Nat Rev Microbiol 17:371–382. https://doi.org/10.1038/s41579-019-0186-5.
7. Miller MB, Bassler BL. 2001. Quorum sensing in bacteria. Annu Rev Microbiol 55:165–199. https://doi.org/10.1146/annurev.micro.55.1.165.
8. Herzog R, Peschek N, Fröhlich KS, Schumacher K, Papenfort K. 2019. Three autoinducer molecules act in concert to control virulence gene expression in Vibrio cholerae. Nucleic Acids Res 47:3171–3183. https://doi.org/10.1093/nar/gky1320.
9. Freeman JA, Bassler BL. 1999. Sequence and function of LuxU: a two-component phosphorelay protein that regulates quorum sensing in Vibrio harveyi. J Bacteriol 181:899–906. https://doi.org/10.1128/JB.181.3.899-906.1999.
10. Freeman JA, Bassler BL. 1999. A genetic analysis of the function of LuxO, a two-component response regulator involved in quorum sensing in Vibrio harveyi. Mol Microbiol 31:665–677. https://doi.org/10.1046/j.1365-2958.1999.01208.x.
11. Lenz DH, Mok KC, Lilley BN, Kulkarni RV, Wingreen NS, Bassler BL. 2004. The small RNA chaperone Hfq and multiple small RNAs control quorum sensing in Vibrio harveyi and Vibrio cholerae. Cell 118:69–82. https://doi.org/10.1016/j.cell.2004.06.009.
12. Papenfort K, Bassler BL. 2016. Quorum sensing signal-response systems in Gram-negative bacteria. Nat Rev Microbiol 14:576–588. https://doi.org/10.1038/nrmicro.2016.89.
13. Bridges AA, Bassler BL. 2019. The intragenus and interspecies quorum-sensing autoinducers exert distinct control over Vibrio cholerae biofilm formation and dispersal. PLoS Biol 17:e3000429. https://doi.org/10.1371/journal.pbio.3000429.

14. Bernier SP, Ha D-G, Khan W, Merritt JH, O'Toole GA. 2011. Modulation of Pseudomonas aeruginosa surface-associated group behaviors by individual amino acids through c-di-GMP signaling. Res Microbiol 162:680–688. https://doi.org/10.1016/j.resmic.2011.04.014.
15. Carlson HK, Vance RE, Marletta MA. 2010. H-NOX regulation of c-di-GMP metabolism and biofilm formation in Legionella pneumophila. Mol Microbiol 77:930–942. https://doi.org/10.1111/j.1365-2958.2010.07259.x.
16. Kanazawa T, Ren S, Maekawa M, Hasegawa K, Arisaka F, Hyodo M, Hayakawa Y, Ohta H, Masuda S. 2010. Biochemical and physiological characterization of a BLUF protein-EAL protein complex involved in blue light-dependent degradation of cyclic diguanylate in the purple bacterium Rhodopseudomonas palustris. Biochemistry 49:10647–10655. https://doi.org/10.1021/bi101448t.
17. Bridges AA, Prentice JA, Fei C, Wingreen NS, Bassler BL. 2022. Quantitative input-output dynamics of a c-di-GMP signal transduction cascade in Vibrio cholerae. PLoS Biol 20:e3001585. https://doi.org/10.1371/journal.pbio.3001585.
18. Tuckerman JR, Gonzalez G, Sousa EHS, Wan X, Saito JA, Alam M, Gilles-Gonzalez M-A. 2009. An oxygen-sensing diguanylate cyclase and phosphodiesterase couple for c-di-GMP control. Biochemistry 48:9764–9774. https://doi.org/10.1021/bi901409g.
19. Ha D-G, O'Toole GA. 2015. c-di-GMP and its effects on biofilm formation and dispersion: a Pseudomonas aeruginosa review. Microbiol Spectr 3:3.2.27. https://doi.org/10.1128/microbiolspec.MB-0003-2014.
20. Waters CM, Lu W, Rabinowitz JD, Bassler BL. 2008. Quorum sensing controls biofilm formation in Vibrio cholerae through modulation of cyclic Di-GMP levels and repression of vpsT. J Bacteriol 190:2527–2536. https://doi.org/10.1128/JB.01756-07.
21. Srivastava D, Harris RC, Waters CM. 2011. Integration of cyclic di-GMP and quorum sensing in the control of vpsT and aphA in Vibrio cholerae. J Bacteriol 193:6331–6341. https://doi.org/10.1128/JB.05167-11.
22. Hammer BK, Bassler BL. 2003. Quorum sensing controls biofilm formation in Vibrio cholerae. Mol Microbiol 50:101–104. https://doi.org/10.1046/j.1365-2958.2003.03688.x.
23. Beyhan S, Bilecen K, Salama SR, Casper-Lindley C, Yildiz FH. 2007. Regulation of rugosity and biofilm formation in Vibrio cholerae: comparison of VpsT and VpsR regulons and epistasis analysis of vpsT, vpsR, and hapR. J Bacteriol 189:388–402. https://doi.org/10.1128/JB.00981-06.
24. Zhou H, Zheng C, Su J, Chen B, Fu Y, Xie Y, Tang Q, Chou S-H, He J. 2016. Characterization of a natural triple-tandem c-di-GMP riboswitch and application of the riboswitch-based dual-fluorescence reporter. Sci Rep 6:20871. https://doi.org/10.1038/srep20871.
25. Bridges AA, Bassler BL. 2021. Inverse regulation of Vibrio cholerae biofilm dispersal by polyamine signals. Elife 10:e65487. https://doi.org/10.7554/eLife.65487.
26. Karatan E, Duncan TR, Watnick PI. 2005. NspS, a predicted polyamine sensor, mediates activation of Vibrio cholerae biofilm formation by norspermidine. J Bacteriol 187:7434–7443. https://doi.org/10.1128/JB.187.21.7434-7443.2005.
27. Casper-Lindley C, Yildiz FH. 2004. VpsT is a transcriptional regulator required for expression of vps biosynthesis genes and the development of rugose colonial morphology in Vibrio cholerae O1 El Tor. J Bacteriol 186:1574–1578. https://doi.org/10.1128/JB.186.5.1574-1578.2004.
28. Yan J, Sharo AG, Stone HA, Wingreen NS, Bassler BL. 2016. Vibrio cholerae biofilm growth program and architecture revealed by single-cell live imaging. Proc Natl Acad Sci U S A 113:E5337–E5343.
29. Hartmann R, Singh PK, Pearce P, Mok R, Song B, Díaz-Pascual F, Dunkel J, Drescher K. 2019. Emergence of three-dimensional order and structure in growing biofilms. Nat Phys 15:251–256. https://doi.org/10.1038/s41567-018-0356-9.
30. Hartmann R, Jeckel H, Jelli E, Singh PK, Vaidya S, Bayer M, Rode DKH, Vidakovic L, Díaz-Pascual F, Fong JCN, Dragoš A, Lamprecht O, Thöming JG, Netter N, Häussler S, Nadell CD, Sourjik V, Kovács ÁT, Yildiz FH, Drescher K. 2021. Quantitative image analysis of microbial communities with BiofilmQ. Nat Microbiol 6:151–156. https://doi.org/10.1038/s41564-020-00817-4.
31. Srivastava D, Waters CM. 2012. A tangled web: regulatory connections between quorum sensing and cyclic di-GMP. J Bacteriol 194:4485–4493. https://doi.org/10.1128/JB.00379-12.
32. De Kievit TR. 2009. Quorum sensing in Pseudomonas aeruginosa biofilms. Environ Microbiol 11:279–288. https://doi.org/10.1111/j.1462-2920.2008.01792.x.
33. Valentini M, Filloux A. 2016. Biofilms and cyclic di-GMP (c-di-GMP) signaling: lessons from Pseudomonas aeruginosa and other bacteria. J Biol Chem 291:12547–12555. https://doi.org/10.1074/jbc.R115.711507.
34. Higgins DA, Pomianek ME, Kraml CM, Taylor RK, Semmelhack MF, Bassler BL. 2007. The major Vibrio cholerae autoinducer and its role in virulence factor production. Nature 450:883–886. https://doi.org/10.1038/nature06284.
35. Semmelhack MF, Campagna SR, Federle MJ, Bassler BL. 2005. An expeditious synthesis of DPD and boron binding studies. Org Lett 7:569–572. https://doi.org/10.1021/ol047695j.
36. Ng W-L, Wei Y, Perez LJ, Cong J, Long T, Koch M, Semmelhack MF, Wingreen NS, Bassler BL. 2010. Probing bacterial transmembrane histidine kinase receptor–ligand interactions with natural and synthetic molecules. Proc Natl Acad Sci U S A 107:5575–5580. https://doi.org/10.1073/pnas.1001392107.
37. Hurley A, Bassler BL. 2017. Asymmetric regulation of quorum-sensing receptors drives autoinducer-specific gene expression programs in Vibrio cholerae. PLoS Genet 13:e1006826. https://doi.org/10.1371/journal.pgen.1006826.
38. Dalia AB. 2018. Natural cotransformation and multiplex genome editing by natural transformation (MuGENT) of Vibrio cholerae, p 8937–8942. *In* Sikora AE (ed), Vibrio cholerae, Methods in molecular biology, vol 1839. Springer, New York, NY.
39. Dalia AB, McDonough E, Camilli A. 2014. Multiplex genome editing by natural transformation. Proc Natl Acad Sci U S A 111:8937–8942. https://doi.org/10.1073/pnas.1406478111.
40. Python Software Foundation. 2022. The Python language reference: Python 3.10.5 documentation. https://docs.python.org/3/reference/. Accessed 21 June 2022.
41. Kim D, Paggi JM, Park C, Bennett C, Salzberg SL. 2019. Graph-based genome alignment and genotyping with HISAT2 and HISAT-genotype. Nat Biotechnol 37:907–915. https://doi.org/10.1038/s41587-019-0201-4.
42. Liao Y, Smyth GK, Shi W. 2014. featureCounts: an efficient general purpose program for assigning sequence reads to genomic features. Bioinformatics 30:923–930. https://doi.org/10.1093/bioinformatics/btt656.
43. Robinson MD, McCarthy DJ, Smyth GK. 2010. edgeR: a Bioconductor package for differential expression analysis of digital gene expression data. Bioinformatics 26:139–140. https://doi.org/10.1093/bioinformatics/btp616.